Incomplete molecular chaos within dense-fluid shock waves

Stefan Schlamp*
Institute of Fluid Dynamics, ETH Zurich, Sonneggstrasse 3, CH-8092 Zürich, Switzerland

Bryan C. Hathorn†
Division of Computer Science and Mathematics, Oak Ridge National Laboratories, Oak Ridge, Tennessee 37831, USA

(Received 12 February 2007; published 22 August 2007)

Large-scale molecular dynamics simulations of an $M_s=4.3$ shock in dense argon ($\rho=532$ kg/m^3, $T=300$ K) and an $M_s=3.6$ shock in dense nitrogen ($\rho=371$ kg/m^3, $T=300$ K) have been performed. The two-point molecular velocity correlation function is calculated within slices in plane with the shock wave. Long-range (~ten molecular radii) positive correlations (correlation coefficient 0.05) are observed for the shock-normal velocity component, the in-plane velocity component, and the rotation rates. No correlations are found upstream or downstream of the shock, indicating that this is a nonequilibrium effect. These correlations violate one of the assumptions underlying the Boltzmann equation.

DOI: 10.1103/PhysRevE.76.026314 PACS number(s): 47.40.−x, 31.15.Qg, 47.61.Cb, 62.50.+p

I. INTRODUCTION

The Boltzmann equation is the appropriate atomistic governing equation in the dilute gas limit. Yet a few underlying assumptions that have to be made to derive it from the Louiville equation are violated for finite densities. Let $f=f(\underline{r},\underline{u},t)$ denote the velocity distribution function, i.e., the number of molecules at $\underline{r}$ and time t that have a velocity $\underline{u}$. Grad [1] summarizes these assumptions.

(1) Point molecules: this is intrinsically implied by writing $f=f(\underline{r},\ldots)$.

(2) Complete collisions: there exists a time interval that is large compared to the duration of a collision, yet small compared to the mean time between collisions.

(3) Slowly varying distribution function: this means that f does not change significantly over the intermediate time scale just mentioned, i.e., $f\approx$const over a distance comparable to the size of a molecule (but not necessarily over the mean free path).

(4) Molecular chaos: the velocities of two molecules with intermolecular distance larger than the range of short-range forces are uncorrelated.

Assumption 1 is correct only in the limit $\delta/\sigma\to\infty$, where δ and σ are the mean distance between molecules and the size of a molecule, respectively. For hard-sphere molecules, the collision event is singular in time such that assumption 2 is always satisfied in this case. For "soft" molecular interactions, however, assumption 2 is more stringent than the assumption of solely binary collisions, which would be satisfied provided that $\sigma\ll\lambda$, where λ is the mean free path.

The thickness of not too weak shock waves is on the order of a few mean free paths. This holds qualitatively for shocks in dilute gases as well as shocks in dense fluids. But because λ is inversely proportional to the density, the shock thickness becomes comparable to σ at high densities. f changes strongly across the shock (reflected by the macroscopic quantities such as density, velocity, temperature) such that its change over a distance σ is not negligible, invalidating assumption 3.

Assumptions 1–3 depend only on the relevant length scales and the validity can thus be evaluated *a priori*. This, however, is not the case for the existence or lack of correlations (assumption 4). It is violated, for example, in fluids near the liquid-vapor critical point, where the behavior of the fluid is dominated by long-range correlations, in shear flows [2–4], for dissipative gases [5], and for high-energy heavy-ion collisions [6]. Here we report on long-range correlations within a shock wave while neither the fluid upstream nor the fluid downstream shows such correlations. We hence demonstrate that each one of assumptions 1–4 is violated within shock waves in dense fluids.

While the current results are not directly transferable to dilute gases, it cannot be ruled out *a priori* that similar correlations also exist within dilute-gas shock waves. While assumptions 1–3 are valid in this regime, the invalidity of assumption 4 would remain.

The next section will first briefly describe the numerical setup before the terminology and data analysis procedure are addressed in Sec. III, followed by the actual results in Sec. IV. The possibility that the observed effect is due to a bias or is a numerical artifact is ruled out in Sec. V, where the results are also interpreted.

II. SETUP

The numerical setup is the same discussed in detail in Ref. [7]. Only the most essential parameters are reproduced here. The molecular dynamics code used is a modified version of MOLDY [8]. The computational domain is a cuboid with dimensions $L_x\times L_y\times L_z=252\times 237.9\times 237.9$ Å^3, where a layer of 15.86 Å thickness on either side (in the x direction) is occupied by a piston and by a stationary wall.

100 000 nitrogen molecules (argon atoms) are randomly distributed within the fluid portion of the domain and given

*Present address: Susquehanna International Group, George's Dock House, IFSC, Dublin 1, Ireland. schlamp@ifd.mavt.ethz.ch; URL: http://www.ifd.mavt.ethz.ch

†hathornb@ornl.gov; URL: http//www.csm.ornl.gov/

random initial velocities and rotation rates drawn from a Maxwell-Boltzmann distribution. The rigid nitrogen molecule is modeled by a two-center Lennard-Jones (6,12) potential with the parameters as given in Ref. [9], but without the five point charges. The argon atom is modeled by a Lennard-Jones (6,12) potential as proposed in Ref. [10]. The mean distance between molecules is $\delta = n^{-1/3} = 5$ Å initially, where n denotes the number density. The mean free path (based on its dilute gas definition and using $2\sigma_{LJ}$ as diameter) is $O(1$ Å$)$.

The system is equilibrated for 2 ps, where the molecular velocities and rotation rates are rescaled periodically to correspond to the desired initial temperature of 300 K. The shock wave is created by impulsively accelerating the left wall (piston) to a velocity of $u_p = 1000$ m/s. The system state is saved every 0.05 ps. Ten ensembles with perturbed initial conditions are simulated. The averaged shock structure is obtained by averaging over all ensembles and over all time steps where the shock wave is at least 50 Å from either wall.

III. DATA ANALYSIS

A. Temporal Averaging

Steady-state data are temporally averaged by mapping the molecular locations onto a shock-fixed coordinate system. The instantaneous location of the shock wave is obtained by a least-squares fit of a Mott-Smith profile [11] to the density field across the domain. While the density profile is not perfectly described by this functional, this approach does provide a reliable method to locate the shock wave accurately. Temporal averaging is performed only while the shock wave is at least 50 Å from either end wall to rule out end wall effects. Seventy (for N_2 69) data sets meet this criterion. Data are analyzed in slices of $\Delta x = 1$ Å thickness such that each slice contains between approximately 300 000 and 600 000 molecules (summed over all ensembles and qualified time steps).

In the shock-fixed frame of reference, flow is from left to right, i.e., the cold side corresponds to $x \to -\infty$ and the hot side is at $x \to +\infty$ (the x direction is reversed from the laboratory-fixed frame of reference). The origin is chosen such that the nondimensional density $(\rho - \rho_1)/(\rho_2 - \rho_1) = 0.5$ (where the subscripts 1 and 2 correspond to the pre- and postshock states, respectively) at $x = x_{s,\rho} = 0$.

B. Correlation coefficient

Let $\underline{x}^i = (x^i, y^i, z^i)$ and $\underline{u}^i = (u^i, v^i, w^i)$ be the location and the velocity vector of molecule i in the shock-fixed reference frame, respectively, where the shock normal is pointing in the $+x$ direction. Further, let $\underline{\Psi}$ be the kinetic state vector of molecule i,

$$\underline{\Psi}^i = (\Psi^i_\perp, \Psi^i_\parallel, \Psi^i_\omega) \equiv (u^i, \sqrt{(v^i)^2 + (w^i)^2}, |\underline{\omega}^i|). \quad (1)$$

The first component is just the shock-normal velocity. The second component is the in-plane velocity magnitude. This makes use of the fact that the in-plane directions are interchangeable and that there cannot be a preferred direction. $|\underline{\omega}|$ is the magnitude of the rotation rate vector, i.e., essentially the square root of the rotational kinetic energy. For the shock wave in argon, only the first two components are relevant. $\underline{\Psi}$ does not have a physical meaning and it does not define the state of a molecule uniquely. It is merely used to simplify the notation.

Let us now define the difference of one molecule's state vector from the local average as

$$\underline{\tilde{\Psi}}^i \equiv \underline{\Psi}^i - \langle \underline{\Psi}^j \rangle, \quad \forall \ j \text{ such that } |x_j - x_i| \le \Delta x/2, \quad (2)$$

where $\Delta x = 1$ Å. This is the excess or deficit relative to all other molecules j within $\Delta x/2$ of molecules i. With this notation, the two-point correlation function is

$$R_{\alpha,\beta}(x,r) \equiv \frac{\langle \tilde{\Psi}^i_\alpha \tilde{\Psi}^j_\beta \rangle}{\sqrt{\langle (\tilde{\Psi}^i_\alpha)^2 \rangle \langle (\tilde{\Psi}^i_\beta)^2 \rangle}}$$

$$\forall \ i \text{ such that } |x^i - x| \le \frac{1}{2}\Delta x,$$

$$\forall \ j \text{ such that } |x^j - x| \le \frac{1}{2}\Delta x, \quad (3)$$

and

$$\left| \sqrt{(y^j - y^i)^2 + (z^j - z^i)^2} - r \right| \le \frac{\Delta r}{2}.$$

The definition is that of a correlation coefficient, except that the averages in the numerator and the denominator go over different groups of molecules. The numerator is the covariance of the state vector of molecules separated by distance r at the shock-normal coordinate x. The average hence goes over all molecules that are within Δx *and* Δr ($\Delta r = 0.2$ Å) of each other. The average in the denominator requires only that molecules are within Δx of each other. In practice, the difference between Eq. (3) and the correlation coefficient will be negligible. Care has to be taken when calculating $R_{\alpha\beta}$ over several time steps and ensembles. The covariance [numerator of Eq. (3)] then has to be calculated for each time step and ensemble separately before summing the results.

IV. RESULTS

Table I summarizes the property changes across the shock waves. A more complete table and plots of the averaged shock structure can be found in Refs. [12,7]. The pressure and the speed of sound do not follow directly from our molecular dynamics MD results, but are calculated from reference-type empirical equations of state suggested by the National Institute of Standards and Technology (NIST) [13,14]. Note that these semiempirical equations of state do not enter the simulation in any way. They are used only to calculate the shock Mach number and the pressures *a posteriori* for indicative purposes. In particular our two-center Lennard-Jones nitrogen model might result in deviations from the behavior of real nitrogen.

The deviation from perfect-gas behavior is most evident from the density ratios, which are approximately 2 for both cases. For perfect-gas shocks with the same Mach numbers

TABLE I. Pre- and postshock conditions of the simulated shock waves in argon and nitrogen.

			Argon		Nitrogen	
	Symbol	Unit	Pre	Post	Pre	Post
Density	ρ	kg/m^3	532.1	1,086.7	370.9	741.0
Temperature	T	K	301.0	1,757.1	300.1	978.0
Pressure	p	MPa	34.12[a]	?	42.3[b]	689.5[b]
Shock speed	u_s	m/s	1,885.0		1,976	
Shock Mach number	M_s		4.28[a]		3.56[b]	
Shock thickness	Λ		8.82[c]		7.47[c]	

[a]Pressure and sound speed are calculated from equation of state of Tegeler *et al.* [14]. The postshock state is out of the range of validity of the equation of state.

[b]Pressure and sound speed are calculated from equation of state of Span *et al.* [13].

[c]Based on the maximum density gradient, i.e., $\Lambda=(\rho_2-\rho_1)/(\partial\rho/\partial x|_{max})$.

and ratios of specific heat, they would be 3.4 and 4.3 for the argon and the nitrogen case, respectively. For a given Mach number, the shock thickness (measured relative to the mean free path) increases with increasing density [15]. The results for the shock thickness are in fact larger by a factor of 2 than those found experimentally in dilute argon [16,17] and dilute nitrogen [16]. The dense-gas effects on the temperature ratios, on the other hand, are weak (Ar: $T_2/T_1=5.9$ instead of 6.6 for a perfect gas; N_2: $T_2/T_1=3.3$ instead of 3.4 for a perfect gas).

The different panels of Fig. 1 show the different components of $R_{\alpha,\beta}(x,r)$ for the $M=3.56$ shock in nitrogen. Note that $R_{\alpha,\beta}=R_{\beta,\alpha}$. The horizontal scale is the shock-normal coordinate normalized by the shock thickness given in Table I. Flow is from left to right, such that the left-hand side of each panel corresponds to the cold side of the shock wave. The vertical scale is the radial distance normalized by the Lennard-Jones radius ($\sigma_{LJ,N_2}=3.318$ Å). The strong repulsive force for small separations results in a minimum spacing of two particles. The vertical scale hence does not start at zero and the white region at the bottom of each panel is a result of this void. Note that this minimum distance is a function of the density and temperature. Closer inspection of Fig. 1 shows that it decreases going downstream across the shock. The strong deviations from zero for the smallest observed spacings (lower edge of the panels) are due to the small number of particle pairs with very small separations and have thus be interpreted as noise. While R can also be negative, no statistically significant negative values have been observed. The color coding thus only covers positive values.

Upstream and downstream of the shock wave, no correlation (discernible from the noise) can be observed for any component of $R_{\alpha,\beta}$. The lower noise levels downstream of the shock wave can be attributed to the higher density there such that more particle pairs fall into each Δx-Δr bin of the histogram. The density ratio is roughly 2 such that the number of molecule *pairs* quadruples. The noise is thus cut in half.

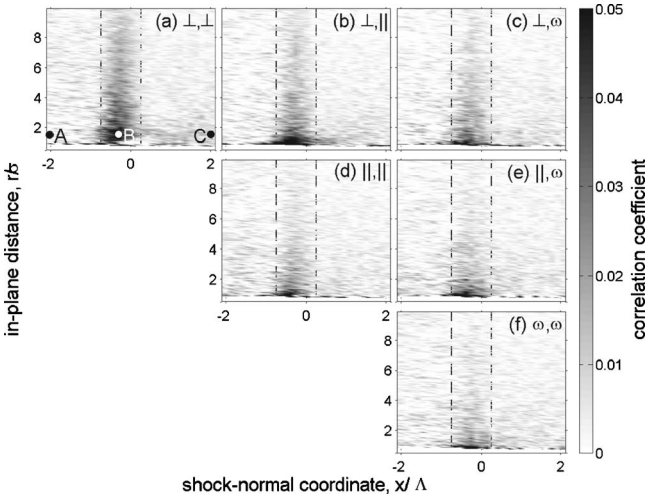

FIG. 1. Two-point velocity correlation functions [Eq. (3)] within a shock in dense nitrogen. The shock-normal coordinate (horizontal scale) is nondimensionalized by the shock thickness Λ. The vertical scale is the in-plane distance between two molecules within the same slice of thickness $\delta x=1$ Å. It is normalized by the Lennard-Jones radius σ. (a) $R_{\perp,\perp}$, (b) $R_{\perp,\parallel}$, (c) $R_{\perp,\omega}$, (d) $R_{\parallel,\parallel}$, (e) $R_{\parallel,\omega}$, and (f) $R_{\omega,\omega}$. The raw data for points *A*, *B*, and *C* shown in Figs. 2(a)–2(c), respectively.

The most significant features of Fig. 1 are the long-range positive correlations visible in each panel. They are centered slightly on the cold side of the shock wave. The vertical dashed lines are plotted at $x/\Lambda=-0.75$ and 0.25 as visual aids. The two-point correlation between the shock-normal velocity is strongest [Fig. 1(a)], but still weak in absolute terms, reaching only ~ 0.05 for small r. $R_{\perp,\perp}>0$ is clearly distinguishable from noise for $r/\sigma=10$ (more than six times the preshock mean distance between molecules). The other components of R deviate less from zero. But, since the correlations exist for all components of R, it is probably more appropriate to speak of long-range correlations of the molecular kinetic energy.

Next we want to address the question if the correlations are produced by just a small fraction of the molecules (or even a few outliers). Figure 2 shows the raw data underlying the three labeled points in Fig. 1(a). Locations *A* and *C* are upstream and downstream of the shock, respectively, while *B* is located where the highest correlation coefficient is observed. Each marker in the upper panels corresponds to the x velocities of a pair of molecules within a slice of thickness $\Delta x=1$ Å centered at $x=-15$ (a), -2 (b), and $+15$ Å (c), and at a distance of $r=10\pm0.1$ Å from each other. Figures 2(a) and 2(c) show a spherically symmetric Boltzmann distribution, as one would expect for thermodynamic equilibrium outside the shock. The larger standard deviation in Fig. 2(c) reflects the higher temperature in the postshock region. Likewise, the higher density there results in a larger sample size. Normally, a doubling of the density would result in a quadrupling of the sample size. Deviations from this ratio are due to the fact that the radial distribution function also

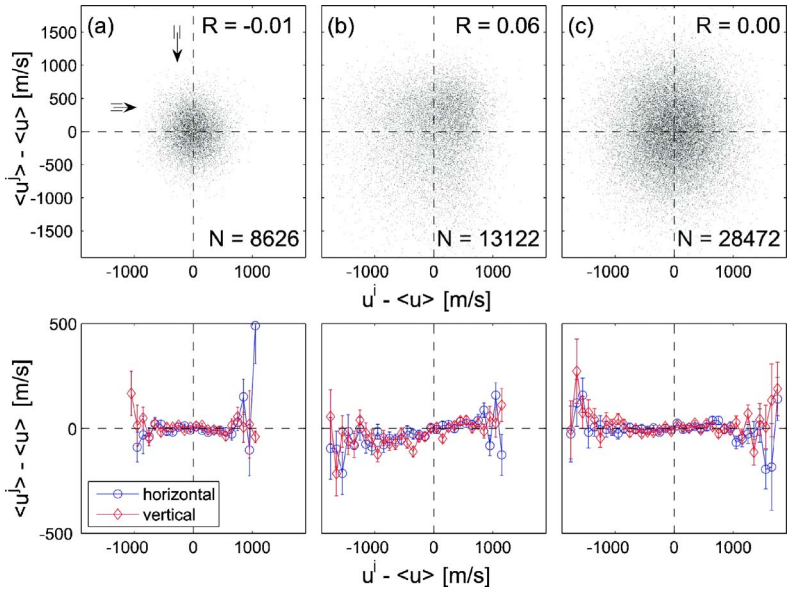

FIG. 2. (Color online) Top panels: raw data at points A, B, and C in Fig. 1(a). When molecules i and j are both within $x\pm\Delta x/2$ and have a distance of $r\pm\Delta r$ from each other, then each dot represents (c^i-u, c^j-u), where c is the shock-normal molecular velocity and u is the mean velocity. R is the correlation coefficient for the data shown and N is the sample size. The bottom panels show the average values along horizontal and vertical slices. Their width is shown in (a).

changes. Figure 2(b) shows the distribution of the relative velocities at a location where the correlations are the strongest. The distribution is not symmetric, but highly skewed (the heat flux is related to the skewness). This alone is not sufficient to explain the correlations and the presence of a correlation is certainly not obvious from looking at the raw data.

The lower panels in Fig. 2 show the averages taken over vertical and horizontal slices in the upper panels. By construction (the assignment of indices i and j is arbitrary), the raw data in the upper panels are symmetric (in a statistical sense) to the +45° diagonal. The two lines in the lower panels should thus coincide. They are both shown (in addition to the error bars for each line individually) to visualize the uncertainty. For the upstream and downstream states, there is no statistically significant deviation from zero. A correlation of the data in the upper panels would be visible as a nonzero slope of the averages in the lower panel. Such a slope is visible only within the shock wave. This slope is not limited to certain regions of the distribution function, but occurs across the entire range of relative velocities. It can thus be concluded that the positive correlation is not a statistical artifact and that it is not due to the behavior of the tails of the velocity distribution function.

Figure 3 shows the analogous results for the $M=4.28$ shock in dense argon. The magnitude of the effect is slightly weaker, but the qualitative behavior is the same as for nitrogen case.

V. DISCUSSION

The presence of velocity, density, and temperature gradients across a finite-thickness slice might potentially lead to a bias. We employ the following procedure to test for such a bias. The in-plane (y^i and z^i) coordinates of the molecules are randomized and $R_{\alpha,\beta}$ is recalculated as before. This preserves all shock-normal gradients while removing any molecular structure such that $R_{\alpha,\beta}=0$ in theory for these randomized data, and, in fact, all correlations observed in Figs. 1 and 3 then vanish. They are thus not due to a systematic bias.

When r is interpreted in a spherical (instead of cylindrical) sense, then correlations would be expected due to the velocity and temperature gradients in the shock-normal direction. Their range would scale with the shock thickness. One would not, however, expect correlations in the homogeneous (parallel to the plane of the shock wave) directions.

Any correlations must be the result of a collision (or, for soft-sphere molecules, interaction) between two molecules or of previous collisions of each with the same third molecule. But note that the thickness of each slice under consideration, $\Delta x=1$ Å, is much thinner than the reach of the correlations $O(10$ Å$)$. The residence time of each molecule within a particular slice is only $\Delta x/u$. This time is much shorter than the mean time required for two molecules to travel the range of the correlations. In general, the collisions that produce the long-range correlations must therefore have happened some

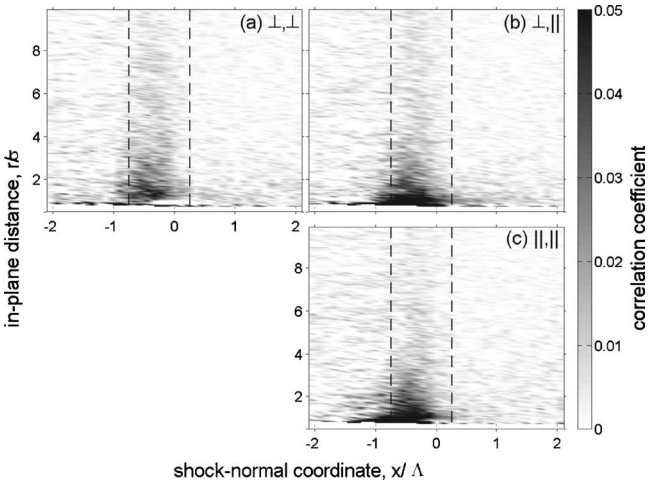

FIG. 3. Same as Fig. 1, but for shock wave in dense argon. (a) $R_{\perp,\perp}$, (b) $R_{\perp,\parallel}$, and (c) $R_{\parallel,\parallel}$.

distance upstream or downstream of the location where the correlations are observed, i.e., outside of the slice where they are observed.

Since the radial distance increases over time and thus—all else being equal—with the shock-normal distance traveled, one would expect that the correlations at large r would correspond to longer times after the collision than the correlations at small r. Assume that molecules A and B collide and suppose they have the same velocity in shock-normal direction after the collision,[1] but that they gradually separate in the in-plane direction over time. Then, unless they travel at the shock speed, their correlation would produce a tilted line in Figs. 1 and 3. Initially, r is small and a corresponding correlation would result near the x location of the original collision. They then move relative to the shock-fixed coordinate system while separating, thereby producing a correlation signature at gradually increasing r as x also changes. Yet the region of correlations in Figs. 1 and 3 is not tilted with respect to the horizontal axis, which would also provide an indication as to where the relevant collision event occurred—upstream or downstream of the observed correlation signature.

The lack of a tilt can then also be interpreted as follows. Correlated molecule pairs travel upstream and downstream in approximately equal numbers. If the correlated pairs were a representative sample of all molecules then one would expect them to be convected downstream on average. This bias is less significant when the correlations are predominantly due to high-energy collisions (i.e., very fast molecules). This would explain not only the lack of a tilt angle, but also the long reach of the correlations.

The likelihood that molecules A and B are both at x some time after the collision is small. Also, over the time it takes the molecules to travel from their interaction site to x, both might interact with several other molecules in their vicinity. Both effects help explain why the observed correlation is so weak.

Another question that has to be answered is why the correlations are not observed throughout the shock, but only in a limited range on the cold side of the shock. One hypothesis is that the higher density (i.e., lower mean free path) toward the hot side of the shock prevents molecules after a collision from separating long distances without interacting with many other molecules along the way. These postcollision interactions would weaken the correlation between the collision partners. Put differently, the shorter mean time between collisions on the hot side of the shock (higher temperature and density) allows for a much quicker equilibration. Finally, we want to point out that the correlations are not due to the high densities *per se*, because neither the preshock nor the postshock state exhibits them.

[1] We effectively only consider collisions where both collision partners have a similar postcollision velocity in the x direction, because only those produce a correlation signature in Figs. 1 and 3.

VI. CONCLUSIONS

In addition to the cases mentioned in the Introduction, we have identified the shock wave as an additional generic flow scenario where the molecular chaos assumption is violated locally—at least for moderately dense fluids. This means that none of the four assumptions underlying the Boltzmann equation is valid in this regime.

The results presented and discussed above provide only two data points (one for each fluid). Questions about the magnitude of the correlations for different densities, temperatures, shock Mach numbers, and pair-interaction potentials thus could not be addressed. The correlations observed here are weak, but other parameters might yield different results. Until results of such parameter studies are available, the validity of the molecular chaos assumption cannot be confirmed *a priori*, but has to be verified *a posteriori*.

Our results expand on the ideas developed by Tsuge [2] and Lutsko [3], who only consider shear flows as examples for translational nonequilibrium. There, it was found that atoms become confined to planes perpendicular to the velocity gradient. This also sheds light on previous results of the authors [12], namely, that anisotropic distributions of the molecular orientations are observed in a shock wave, and offers an alternative mechanism underlying this phenomenon.

A question of particular interest is if similar correlations can be observed in the dilute-gas limit. If so, then the use of the Boltzmann equation might not be fully justified even though assumptions 1–3 hold. It has to be said that experimental shock structure data agree well with DSMC results [18], such that any error is probably irrelevant for engineering purposes. In fact, even a modified treatment of the Navier-Stokes equations yields very good results [19], and the largest remaining discrepancy is observed on the hot side of the shock, whereas the correlations are most pronounced toward the cold side.

ACKNOWLEDGMENTS

This work was sponsored by the Division of Computer Science and Mathematics and used resources of the Center for Computational Sciences at Oak Ridge National Laboratory, which is supported by the Office of Science of the U.S. Department of Energy under Contract No. DE-AC05-00OR22725.

[1] H. Grad, Commun. Pure Appl. Math. **2**, 331 (1949).
[2] S. Tsuge, Phys. Lett. **36A**, 249 (1971).
[3] J. F. Lutsko, Phys. Rev. Lett. **77**, 2225 (1996).
[4] J. J. Erpenbeck, Phys. Rev. Lett. **52**, 1333 (1984).
[5] T. Pöschel, N. V. Brilliantov, and T. Schwager, Int. J. Mod. Phys. C **13**, 1263 (2002).
[6] K. Tamosiunas, L. P. Csernai, V. K. Magas, E. Molnar, and A. Nyiri, J. Phys. G **31**, S1001 (2005).

[7] S. Schlamp and B. C. Hathorn, J. Comput. Phys. **223**, 305 (2007).
[8] K. Refson, Comput. Phys. Commun. **126**, 310 (2000).
[9] C. S. Murthy, S. F. O'Shea, and I. R. McDonald, Mol. Phys. **50**, 531 (1983).
[10] J. Vrabec, J. Stoll, and H. Hasse, J. Phys. Chem. B **105**, 12126 (2001).
[11] H. M. Mott-Smith, Phys. Rev. **82**, 885 (1951).
[12] S. Schlamp and B. C. Hathorn, Phys. Fluids **18**, 096101 (2006).
[13] R. Span, E. W. Lemmon, R. T. Jacobsen, W. Wagner, and A. Yokozeki, J. Phys. Chem. Ref. Data **29**, 1361 (2000).
[14] C. Tegeler, R. Span, and W. Wagner, J. Phys. Chem. Ref. Data **28**, 779 (1999).
[15] J. M. Montanero, M. Lopez de Haro, A. Santos, and V. Garzo, Phys. Rev. E **60**, 7592 (1999).
[16] M. Linzer and D. F. Hornig, Phys. Fluids **6**, 1661 (1963).
[17] M. Camac, Phys. Fluids **7**, 1076 (1964).
[18] D. A. Erwin, G. C. Pham-Van-Diep, and E. P. Muntz, Phys. Fluids A **3**, 697 (1991).
[19] B. L. Holian, C. W. Patterson, M. Mareschal, and E. Salomons, Phys. Rev. E **47**, R24 (1993).